We are IntechOpen, the world's leading publisher of Open Access books Built by scientists, for scientists

6,900
Open access books available

186,000
International authors and editors

200M
Downloads

Our authors are among the

154
Countries delivered to

TOP 1%
most cited scientists

12.2%
Contributors from top 500 universities

CLARIVATE ANALYTICS
BOOK CITATION INDEX
INDEXED

WEB OF SCIENCE™

Selection of our books indexed in the Book Citation Index
in Web of Science™ Core Collection (BKCI)

Interested in publishing with us?
Contact book.department@intechopen.com

Numbers displayed above are based on latest data collected.
For more information visit www.intechopen.com

Real-Time Processing of 3D-TOF Data in Machine Vision Applications

Stephan Hussmann, Torsten Edeler and Alexander Hermanski
Institute for Machine Vision Technology (Ma.Vi.Tec),
West Coast University of Applied Sciences
Germany

1. Introduction

In machine vision applications, Time-of-Flight (TOF) sensors like the Photonic Mixer Devices (PMD Technologies [PMD], 2011) became considerable alternatives to common 3D sensing devices. Because of the enormous progress in TOF-vision systems, nowadays 3D matrix cameras can be used for many applications such as robotic, automotive, industrial, medical and multimedia applications. Due to the increasing demand of safety requirements in the automotive industry it can be assumed that the TOF-camera market will grow and the unit price of these systems in the mass production will drop down to ca. 100 € (Hussmann & Hess, 2006).

Many 3-D sensing techniques have been developed in the past decades. A good review can be found in (Jarvis, 1983). 3-D sensing methods can be divided into several categories:

1. *Shape-from Techniques*: These monocular approaches recover relative depth from texture, from shading, from contours, from motion, etc.; resulting in surface orientations with respect to a viewer-centered coordinate system (Hu & Stockman, 1989). These techniques must deal with correspondence problems. Furthermore problems arise due to the uncertainty of the position at which each image is taken and due to dynamic changes that may occur in the time between two images.
2. *Stereo*: This method simulates the two eyes of a human. It uses multiple visual sensors (two cameras, for example) to estimate stereo disparity and then recover depth (Hu & Stockman, 1989). Stereo cameras introduce physical restrictions due to the need for camera separation. Further, stereo cameras depend on texture matching from both camera images for range estimation. This produces a rather sparse and unevenly distributed data set. Due to the allocation problem dynamic tracking of objects is not an easy task (Hussmann & Liepert, 2009).
3. *Structured Light*: In illuminating the scene, natural ambient light is replaced by an artificial light source, which can be of any structure (pattern) that is convenient for the task. Using structured light by itself is not an independent approach to 3-D sensing; the underlying means is still a monocular (shape-from) or binocular (stereo) method, but under different illumination conditions and hence facing rephrased problems. If a single light beam or a single light plane is used as the light source, the underlying method is direct sensing through triangulation. If a uniform grid of light is the light source, the underlying method is stereo and analysis of textures and contours. The

major advantage of using structured light over ambient light is that features in the images are better defined. Image features are easier to detect; their relationships are more regular (parallel, equi-spaced, etc.) following the property of the generating pattern of the light source; and they prominently reveal the surface geometry that humans can readily use to interpret the scene (Hu & Stockman, 1989).

4. *Direct Sensing* (time-of-flight): One representative of this approach is a laser range finder, which can sense the depth to any surface point in its field of view. Laser range finders are often used for navigation tasks (Nuechter et al., 2003). The major disadvantage of these systems is the use of mechanical components and that they do not deliver 2D intensity images and range data at the same time. Another representative are TOF cameras (Blanc et al., 2004 ; Schwarte et al., 1997), which combine the advantage of active sensors and camera based approaches as they provide a 2D image of intensity and exact distance values in real-time. They do require a synchronized light source. Compared to *Shape-from Techniques* and *Stereo* TOF cameras can deal with prominent parts of rooms like walls, floors, and ceilings even if they are not structured. In addition to the 3D point cloud, contour and flow detection in the image plane yields motion information that can be used for e.g. car or person tracking (Hussmann et al., 2008). *Structured light* applications can have a higher measurement accuracy as TOF-cameras, however the measurement range is then limited.

Inspection task in machine vision applications e.g. quality control of bulk materials are very complex due to their real-time requirements. New accurate and fast algorithms for 3D object recognition and classification are needed as the inspection time is always decreasing. As now commercial 3D-TOF cameras are available at a reasonable price the number of machine vision applications using this technology is expected to increase significantly. Hence in this book chapter the use of 3D-TOF cameras for machine vision applications is investigated.

The state of the art is to use a four-phase shift algorithm for TOF cameras to correctly determine the range value (Blanc et al., 2004; Lange & Seitz, 2001; Ringbeck & Hagebeuker, 2007). The optical signal is sampled four times per period at equidistant intervals. The corresponding sampling points permit unique determination of all relevant parameters of the incoming optical echo's waveform. The sample points are not acquired during only a single period but summed over several hundreds or thousands of periods, which considerably increases the signal-to-noise ratio and hence, finally, the accuracy of the measurement. Due to acquisition of the four subsequent phase images, fast object motion leads to distance uncertainties in situations where corresponding phase images do not properly align with respect to object points.

In (Hussmann & Edeler, 2010) we presented a pseudo-four-phase-shift algorithm for 3D-TOF photonic mixer device (PMD) cameras, which only has to capture two phase images and thereby doubles the frame rate. Hence distance uncertainties by fast moving objects will be reduced. In (Hussmann et al., 2011a) we presented a simple motion compensation algorithm for constant lateral motion such as measure objects on a conveyor belt, which can be processed with the maximum frame rate of currently available commercial TOF cameras. However this algorithm was based on the state of the art 4-phase shift algorithm.

In this book chapter we will combine the two proposed algorithms and evaluate their performance in comparison to the state-of-the-art algorithm. The book chapter is structured as follows. In section 2 we derive the basics of PMD TOF vision systems and subsequently

present algorithms used for real-time processing of PMD TOF data. In section 3 experiments are conducted to investigate the real-time performance of the proposed algorithm for machine vision applications. Concluding remarks will summarize the chapter.

2. Real-time processing of PMD TOF data

2.1 Operating principle of PMD TOF sensors

Fig. 1 shows the cross section of a typical PMD pixel comprising two symmetrical, transparent photo gates. The photons of the received optical echo P_{opt} enter the p-doped substrate through these gates and are generating charge carrier (electron/hole-pairs). The gates are isolated from the p-doped substrate by a SiO_2 - or Si_3N_4 – isolation layer (channel stop) and bounded on the left and right side by n^+ - diffusion readout gates. The photo gates are controlled by the modulation voltage u_m and the offset voltage U_0. The schematic potential distribution in the p-doped substrate between the photo gates is shown in Fig. 1 for a negative modulation voltage u_m.
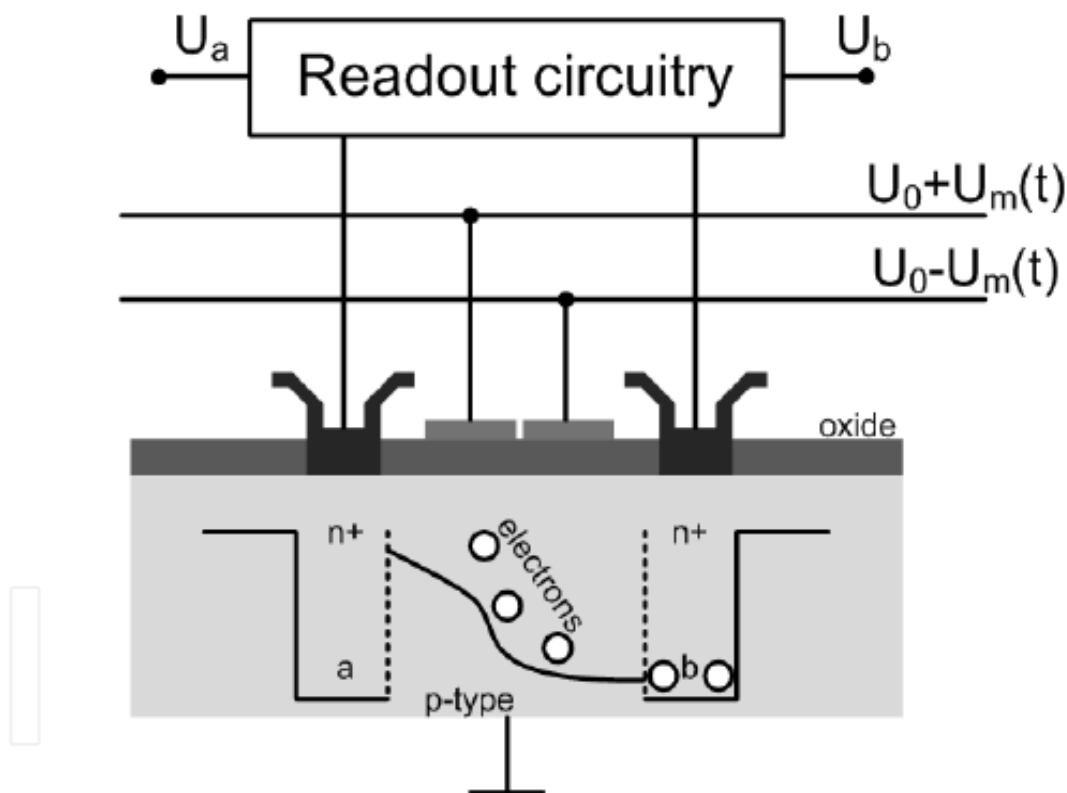

Fig. 1. Cross section of a typical PMD pixel

A PMD pixel may be understood as a modulation controlled photo charge distributer (photonic mixer). In principle the PMD pixel works like a seesaw for electrons while controlling its motion by means of polarity and slope of the seesaw. If no modulated light is received the photo generated charges symmetrically drift to both readout gates a and b. If modulated light is received the photo generated charges drift only to readout gate b, when the modulated light and the modulation voltage have a phase difference of 180° (see Fig. 1). If the phase difference is 0° the photo generated charges drift only to readout gate a.

State of the art is to use continuous wave (CW) modulation with square waves for TOF cameras with a typical modulation frequency of 20 MHz (Hussmann et al., 2008). Hence the modulation voltages can be easily generated digitally with a high accuracy and stability using programmable logic devices (PLDs) such as complex programmable logic devices (CPLD) or field programmable gate arrays (FPGA). For the illumination source infrared (IR) - light emitting diodes (LEDs) are used. The low-pass characteristic of the IR-LEDs leads to an attenuation of the square waves' harmonics for larger frequencies. This results in an optical output that gradually looks sinusoidal for frequencies larger than 5-10 MHz (see Fig. 2). This has to be taken into account if CW modulation with square waves is used.
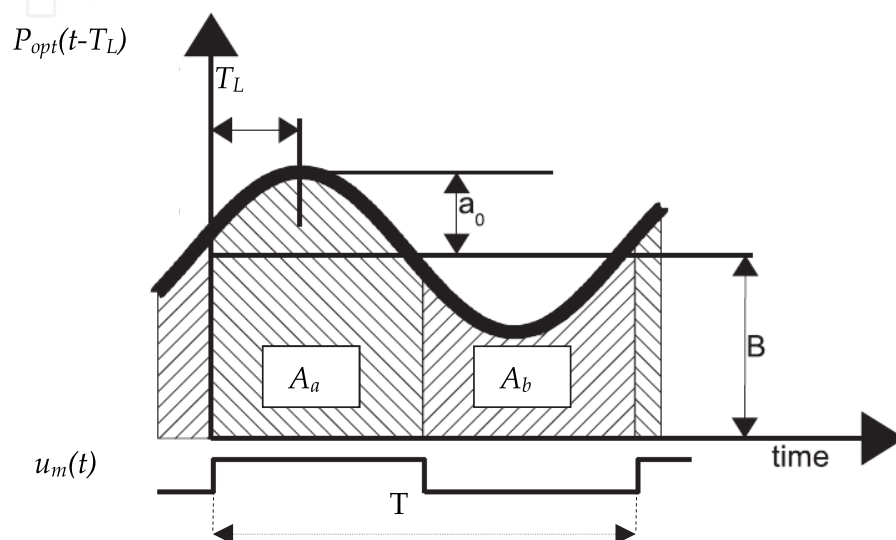

Fig. 2. Correlation process between the received optical echo P_{opt} and the modulation voltage u_m for a single modulation period

The readout gates a and b are each connected to an integration capacitor. Hence the corresponding voltages U_a and U_b can be expressed as a correlation function between the optical echo $P_{opt}(t\text{-}T_L)$ and the modulation voltage $u_m(t)$ over the integration time T_{int}. Fig. 2 illustrates the correlation process for one single modulation period T for the two signals $P_{opt}(t\text{-}T_L)$ and $u_m(t)$. The modulation voltage $u_m(t)$ and the optical echo $P_{opt}(t\text{-}T_L)$ are defined as follows:

$$u_m(t) = \begin{cases} 1, & \text{for } 0 \leq \text{t-N} \cdot \text{T} \leq \text{T}/2 \\ 0, & \text{for } \text{T}/2 < \text{t-N} \cdot \text{T} \leq \text{T} \end{cases} , \quad N = 0,1,2\ldots \tag{1}$$

$$P_{opt}(t - T_L) = a_0 \cdot \cos(\omega t - T_L) + B \tag{2}$$

T_L is the 'time-of-flight' time for the light (camera-object-camera), B is the received average incident light (background light and DC component of the modulated light source) and a_0 is the amplitude of the received modulated light. U_a and U_b are then proportional to the areas A_a and A_b as shown in Fig. 2. If the complete integration time T_{int} (corresponds to several hundreds or thousands of periods) has taken into account, U_a and U_b can be written as:

$$U_a(T_L) = K \cdot \int_0^{T_{int}} P_{opt}(t - T_L) \cdot u_m(t)dt = K \cdot \frac{T_{int}}{T}\left[\frac{T \cdot a_0}{\pi}\sin(T_L) + \frac{T \cdot B}{2}\right] = K \cdot \frac{T_{int}}{T} \cdot A_a(T_L) \tag{3}$$

and

$$U_b(T_L) = K \cdot \int_0^{T_{int}} P_{opt}(t - T_L) \cdot u_m(t - T/2)dt = K \cdot \frac{T_{int}}{T}\left[-\frac{T \cdot a_0}{\pi}\sin(T_L) + \frac{T \cdot B}{2}\right] = K \cdot \frac{T_{int}}{T} \cdot A_b(T_L) \quad (4)$$

The conversion gain K converts the received optical energy into a voltage. The integration time T_{int} does not have to be necessarily a multiple of the single period time T as the number of periods integrated over the integration time is in the range of hundreds to thousands. Looking at Fig. 2 it can be noticed that U_a and U_b are always a positive voltage. To remove the influence of the background light B the difference of ΔU_{ab} has to be determined:

$$\Delta U_{ab}(T_L) = U_a - U_b = K \cdot \frac{T_{int}}{T} \cdot \left(A_a(T_L) - A_b(T_L)\right) \quad (5)$$

The autocorrelation function ΔU_{ab} corresponds to the distance value of a PMD pixel. The sum of U_a and U_b corresponds to all received and converted photons. Hence this sum is equivalent to the grey level value of standard CCD/CMOS video cameras (amplitude image):

$$\sum U_{ab} = U_a + U_b = K \cdot \frac{T_{int}}{T} \cdot (A_a + A_b) = K \cdot \int_0^{T_{int}} P_{opt}(t - T_L)dt = B \quad (6)$$

It has to be mentioned that in this book chapter only infrared light is used as an IR-filter is mounted on top of the sensor chip. Using an IR-filter reduces the effects of the background illumination B on the distance resolution. Hence the amplitude image in this book chapter could be also called "infrared amplitude image". However without the IR-filter the TOF camera would behave like a standard 2D-camera and therefore we still use the word "amplitude image".

Equation (5) and (6) demonstrate the advantage of the PMD technology compared to other 3-D sensing techniques. The PMD pixel is a TOF vision system with inherent suppression of uncorrelated light signals such as sun light or other modulated light disturbances (neon tubes, high frequency illumination modules etc.). More advantages of a PMD TOF vision system are the acquisition of the amplitude value and range data in each pixel without high computational cost and any moving components as well as the monocular setup.

2.2 State-of-the-art range image calculation using 4-phase shift algorithm

As mention in the last section the range value corresponds to ΔU_{ab}. The amplitude of the received optical echo P_{opt} varies with the measure object reflectivity coefficient and the distance. Hence the amplitude of the output voltage ΔU_{ab} is also affected by these changes. To overcome the amplitude dependency of the output voltage of ΔU_{ab} state of the art is to use a 4-phase shift algorithm (Blanc et al., 2004; Lange & Seitz, 2001; Ringbeck & Hagebeuker, 2007). In (Hussmann & Liepert, 2009) the following equation to calculate the phase difference φ_0 without any dependency on the received optical echo's amplitude is derived:

$$\varphi_0 = \arctan\left(\frac{\Delta U_{ab}(270°) - \Delta U_{ab}(90°)}{\Delta U_{ab}(0°) - \Delta U_{ab}(180°)}\right) \quad (7)$$

The range value R can now be calculated by taken into account the modulation frequency f_{mod} and the physical constant for the speed of light c ($3 \cdot 10^8$ m/s). N represents the ambiguity in range estimation when $\varphi_0 > N \cdot 360°$. For example if a modulation frequency of 20 MHz is used the ambiguity range is 7,5 m. If the distance to an object is now 9 m, $N = 1$ and the distance measured by the camera is 1.5 m.

$$R = \frac{c}{2 \cdot f_{\mathrm{mod}}} \cdot \left(\frac{\varphi_0}{360°} - N \right) \; with \; N = 0,1,2,3... \tag{8}$$

2.3 Real-time range image calculation using pseudo 4-phase shift algorithm

Looking at equation (3) and (4) it can be noticed that U_a and U_b have a phase difference of 180° (T/2) to each other:

$$U_a(T_L + \frac{T}{2}) = K \cdot \frac{T_{\mathrm{int}}}{T} \left[\frac{T \cdot a_0}{\pi} \sin(T_L + \frac{T}{2}) + \frac{T \cdot B}{2} \right] = K \cdot \frac{T_{\mathrm{int}}}{T} \left[-\frac{T \cdot a_0}{\pi} \sin(T_L) + \frac{T \cdot B}{2} \right] = U_b(T_L) \tag{9}$$

Hence the output voltage ΔU_{ab} can be expressed as:

$$\Delta U_{ab}(T_L) = U_a(T_L) - U_b(T_L) = U_a(T_L) - U_a(T_L + T/2) \tag{10}$$

Equation (10) shows that a PMD pixel delivers two phase values ($U_a(T_L)$ and $U_a(T_L+T/2)$) at one image capture. Therefore equation (7) can be simplified to:

$$\varphi_0 = -\arctan\left(\frac{\Delta U_{ab}(90°)}{\Delta U_{ab}(0°)} \right) \tag{11}$$

The range value R can now be calculated by using equation (8). Equation (11) demonstrates the advantage of the pseudo 4-phase shift algorithm. Only two image captures instead of four are required to calculate the phase difference φ_0. Hence the frame rate of PMD TOF sensors is doubled without changing the integration time T_{int}. A typical frame rate of TOF PMD cameras is 50 Hz. The pseudo 4-phase shift algorithm increases this frame rate to 100 Hz and hence is well suited for real-time machine vision applications. A more detailed description of the pseudo 4-phase shift algorithm can be found in (Hussmann & Edeler, 2010).

2.4 Real-time arctangent calculation using a reconfigurable processor system

The most time critical operation of the phase difference φ_0 calculation is the arctangent function (see equation (7) and equation (11)). As the arctangent function is called for each individual pixel to determine the range value, the processing time increases with the number of present pixels. The hardware algorithm proposed in (Hussmann et al., 2011b) to calculate the arctangent value for 3D-TOF PMD cameras in real-time is realized as a custom functional unit on the reconfigurable functional unit (RFU) of a reconfigurable processor in a FPGA. This algorithm replaces the state-of-the-art CORDIC arctangent function commonly used in microcontrollers. This significantly decreases the processing time to determine the range image of the 3D vision system.

As the arctangent function is symmetrical only the angles from zero to ninety degree have to be calculated. A further reduction of the angle range down to 45° can be achieved by taken into account the following:

$$\varphi_0 = \begin{cases} \arctan\left(\dfrac{y_0}{x_0}\right), & \text{for } y_0 \leq x_0 \\ 90° - \arctan\left(\dfrac{x_0}{y_0}\right), & \text{for } y_0 > x_0 \end{cases} \tag{12}$$

With a desired range resolution of 1 mm (equivalent to an angle resolution of 0.048°) and an angle range of 45°, a LUT with 2048 elements is needed. As shown in table 1 this LUT is filled with the distance values of the according phase angles. As can be seen in table 1 the distance resolution between each LUT entry is smaller than 1 millimeter. Furthermore it can be seen that at the end of the LUT the distance resolution is better as at the start of the LUT.

i	tan(angle) = i / 2048	angle in degree	distance in mm
0	0	0	0
1	0.000488	0.027976	0.6
2	0.000977	0.055953	1.2
3	0.001465	0.083929	1.7
4	0.001953	0.111906	2.3
5	0.002441	0.139882	2.9
6	0.002930	0.167858	3.5
7	0.003418	0.195834	4.1
8	0.003906	0.223811	4.7
9	0.004395	0.251786	5.2
…			
2042	0.997070	44.915948	935.7
2043	0.997559	44.929973	936.0
2044	0.998047	44.943992	936.3
2045	0.998535	44.958005	936.6
2046	0.999023	44.972010	936.9
2047	0.999512	44.986008	937.2

Table 1. Lookup table of the hardware algorithm

Looking at equation (12) a comparator, a hardware divider, a subtraction device and a LUT is needed to determine the distance value. The comparator checks if $y_0 > x_0$, the hardware divider calculates y_0 / x_0 or x_0 / y_0 depending on the comparator result, the division result is used as index for the LUT and finally the LUT delivers, depending on the comparator result,

the distance value directly or this value has to be subtracted from the distance value 1.875 m (equivalent to 90°).

The hardware algorithm and the state-of-the-art CORDIC algorithm is implemented into a FPGA (Altera Stratix EP1S10F780C6) using a clock frequency of 50 MHz. Therefore the CORDIC algorithm takes 340 ns and the proposed hardware algorithm 160 ns respectively for a standard arctangent calculation. Compared to the execution time of 800 μs for the arctangent C-function *atan2()* from the "math.h" library on the NIOS II processor, a speed-up factor of 2,353 for the CORDIC algorithm and 5,000 for the proposed hardware algorithm is achieved. Hence the total processing time of one range image of a TOF camera with 204 x 204 pixels (PMD[vision]® CamCube 2.0) takes for the CORDIC algorithm 14.15 ms and for the proposed hardware algorithm 6.66 ms respectively.

The maximum frame rate of the used commercial camera (PMD[vision]® CamCube 2.0) is 25 fps, which corresponds to a capture time of 40 ms per image. Using the proposed algorithm with the total processing time for the arctangent function of 6.66 ms leaves enough time to process the range calculation in real-time. To our knowledge there is no other hardware algorithm with the same performance. The proposed approach will significantly reduce the system costs of TOF cameras as state-of-the-art is to use high performance microcontroller in combination with a FPGA. This is an important achievement as the current 3D TOF cameras are too expensive for common machine vision applications. A more detailed description of the hardware algorithm can be found in (Hussmann et al., 2011b).

2.5 Real-time motion artifact compensation

Distance uncertainties typically occur where objects or the camera itself move while the consecutive phase images are taken. They arise from unmatched phase values during the demodulation process. The faster the objects move or the higher the integration time the higher are the distance uncertainties. In (Hussmann et al., 2011a) a compensation algorithm for constant lateral motion is proposed as this is a typical motion in machine vision applications. One industrial example is 3D dimension measurement of objects on a conveyor belt (luggage handling systems, quality control of food or beverages etc.).

The lateral motion of objects on a conveyor belt has to be corrected in only one direction (moving direction of the conveyor belt). This can be done by subtracting the captured amplitude images $\Sigma U_{ab}(0°)$, $\Sigma U_{ab}(90°)$, $\Sigma U_{ab}(180°)$ and $\Sigma U_{ab}(270°)$, and subsequent thresholding using a fixed threshold s to get the binary image B_1-B_3:

$$B_n = \left| \Sigma U_{ab}(0°) - \Sigma U_{ab}(n \cdot 90°) \right| > s \quad , \text{with } n = 1,2,3 \tag{13}$$

Fig. 3 shows typical binary images of an object moving on a conveyor belt. It can be seen that the width of the white area increases linear with the capture time. To compensate the motion the width of the area has to be determined and the amplitude images have to be moved accordingly before the distance image is calculated. The proposed method is computational not expensive and can be easily integrated into an FPGA as shown in (Hussmann et al., 2011a). Hence the motion compensation can be realized in real-time. It has to be noticed that the sensor must be calibrated to make sure that every pixel has a uniform behaviour when exposed with the active light source of the TOF camera (multiplicative

shading calibration). A more detailed description of the motion artefact compensation algorithm and the calibration method can be found in (Hussmann et al., 2011a).

imgBin0min90

imgBin0min180

imgBin0min270

motion direction
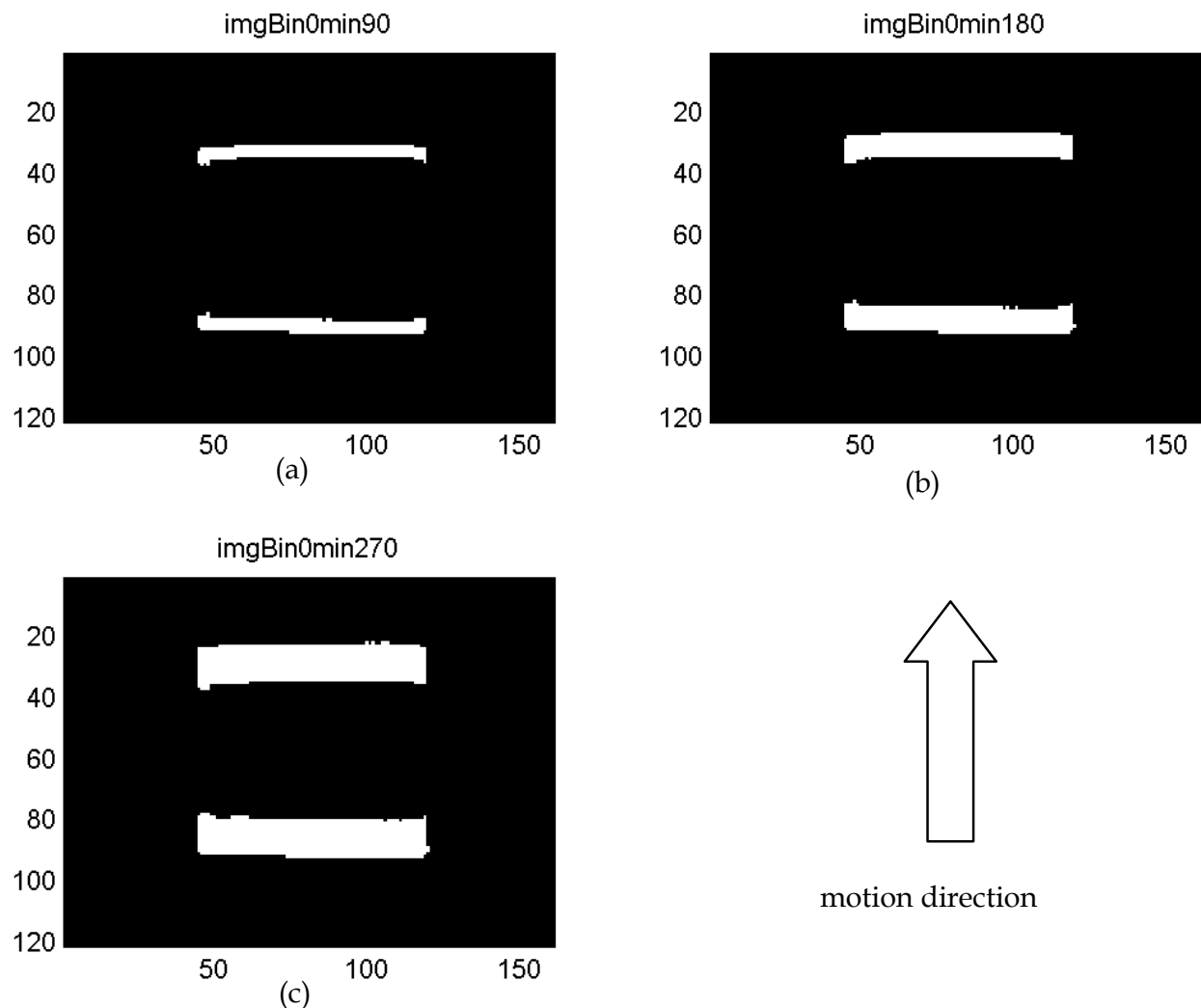
Fig. 3. Binarized difference images of the application in section 3
(a) Binary image of difference image $\Sigma U_{ab}(0°)-\Sigma U_{ab}(90°)$
(b) Binary image of difference image $\Sigma U_{ab}(0°)-\Sigma U_{ab}(180°)$
(c) Binary image of difference image $\Sigma U_{ab}(0°)-\Sigma U_{ab}(270°)$

3. Experiments

3.1 Experimental setup

In Fig. 4 the laboratory setup is shown. A measure object (10 cm x 10 cm x 12 cm) is placed on a conveyor belt, which runs at a speed of 1 m / s. A PMD TOF camera (PMD[vision]® CamCube 2.0) with 204 x 204 pixels is placed 103 cm above the conveyor belt. The raw data (U_a and U_b) of the PMD camera for the four different phases τ ($\tau = 0°$, $\tau = 90°$, $\tau = 180°$ and $\tau = 270°$) are captured and the proposed motion compensation algorithm in (Hussmann et al., 2011a) combined with the pseudo-four-phase-shift algorithm proposed in (Hussmann & Edeler, 2010) is investigated offline using Matlab.

Fig. 4. Laboratory setup

3.2 Experimental results

Fig. 5 shows the amplitude images of the four different phases. The amplitude image is calculated using equation (6). The displacement of the measure object is difficult to notice hence the subtraction results between the different amplitude images are shown in Fig. 6.

The displacement of the object during the acquisition of the four phase images can be clearly seen in Fig. 6. After thresholding and moving of the phase images as proposed in section 2.5, the corrected distance image can be calculated.
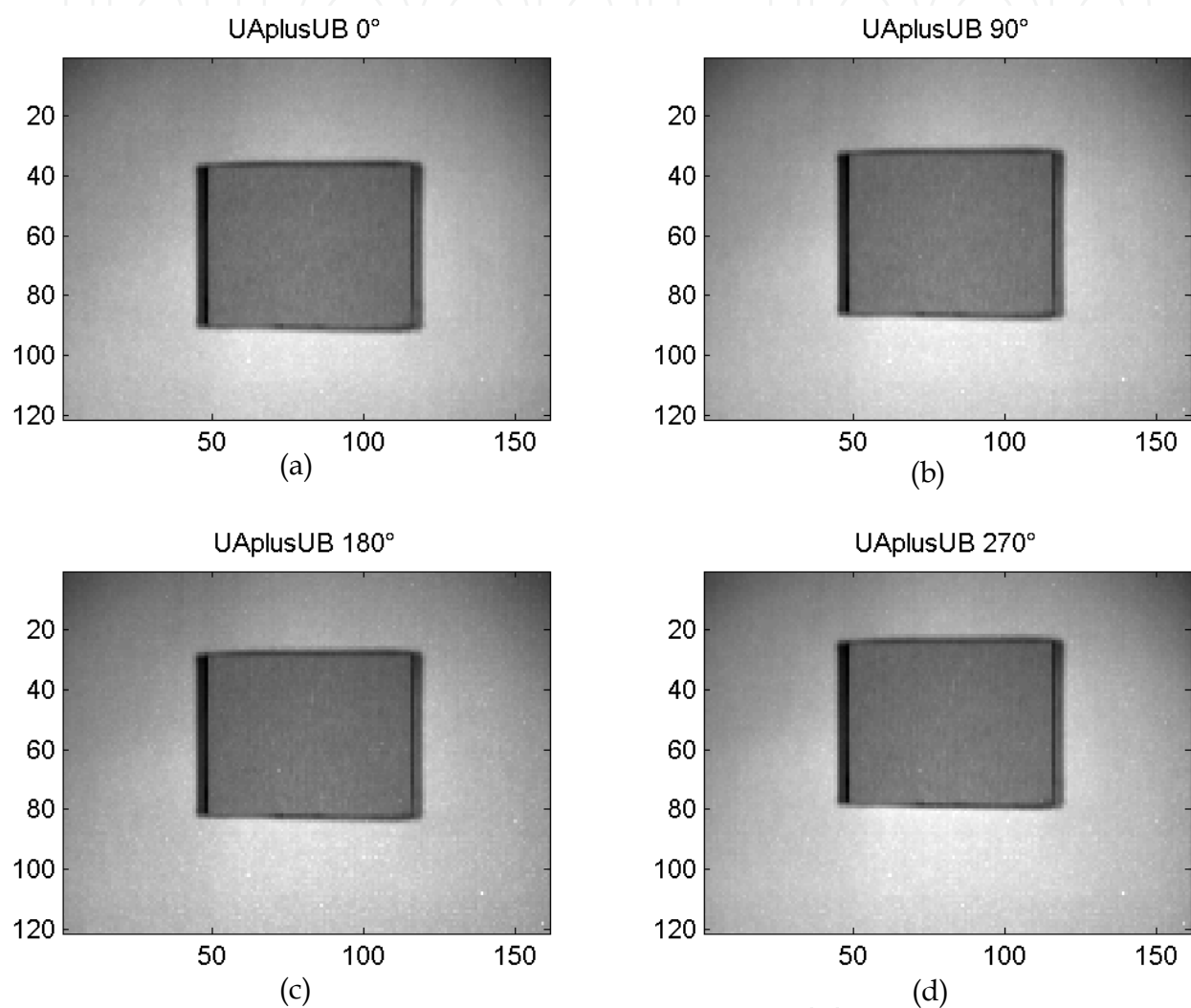
Fig. 5. Amplitude images of the four different phases:
(a) Amplitude image of $\Sigma U_{ab}(0°)$ ("ground truth")
(b) Displaced amplitude image of $\Sigma U_{ab}(90°)$
(c) Displaced amplitude image of $\Sigma U_{ab}(180°)$
(d) Displaced amplitude image of $\Sigma U_{ab}(270°)$

Fig. 7 – Fig. 10 illustrate the influence of the calibration method and the motion artefact compensation algorithm proposed in (Hussmann et al., 2011a) on the distance image using the state-of-the-art 4-phase shift algorithm and the pseudo 4-phase shift algorithm proposed in (Hussmann & Edeler, 2010) respectively. Fig. 7 shows the distance image without motion

compensation using the state-of-the-art 4-phase shift algorithm. It can be seen that the distance at the object edges are not calculated correctly (area 1 and area 3) and that the standard deviation is larger than in the other areas (see table 2). Furthermore it can be noticed that the distance image in Fig. 7 (a) is noisier than in Fig. 7 (b) due to the calibration method proposed in (Hussmann et al., 2011a).
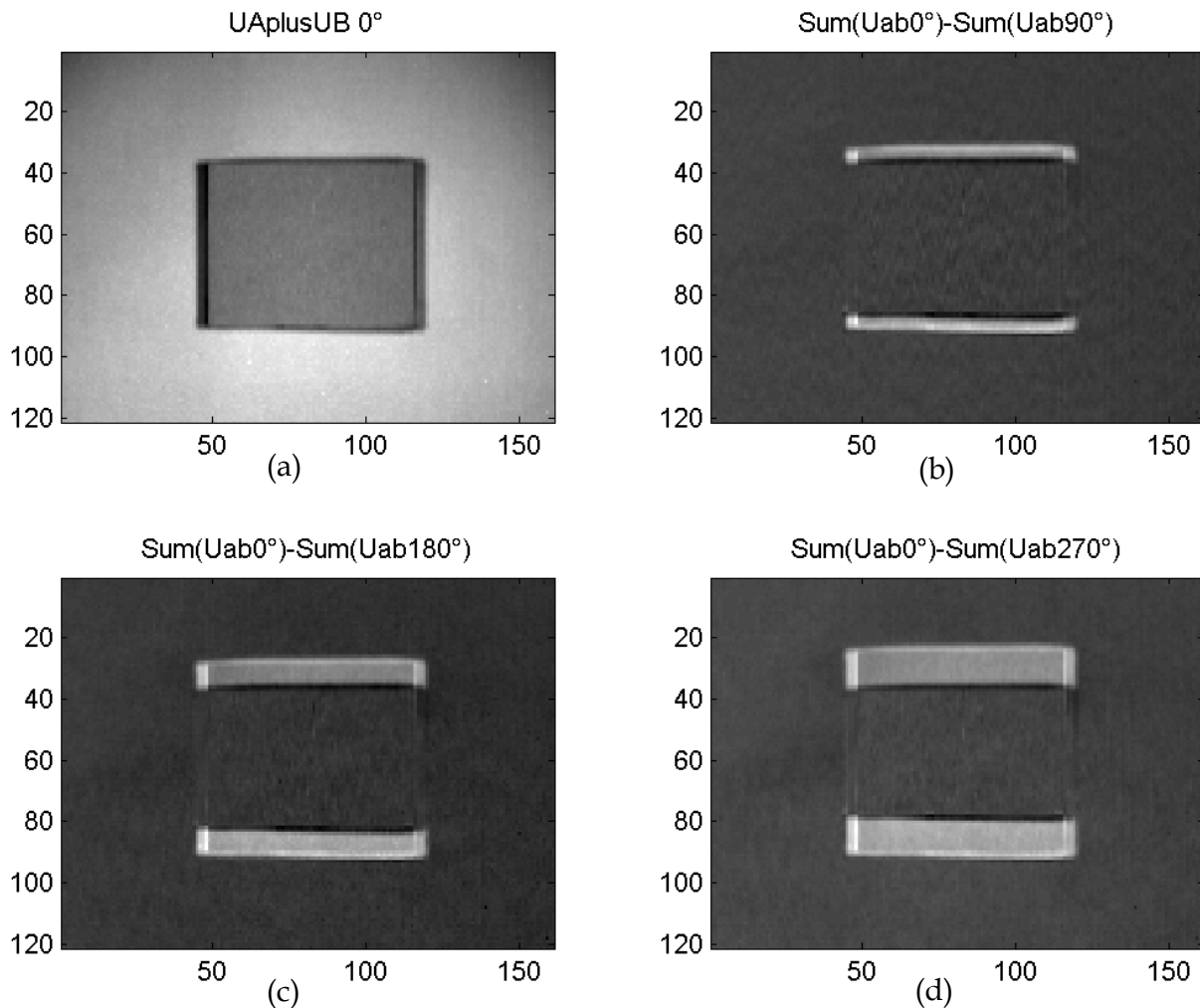

Fig. 6. Subtraction results of the amplitude images:
(a) Amplitude image of $\Sigma U_{ab}(0°)$ ("ground truth")
(b) Difference image $\Sigma U_{ab}(0°)$-$\Sigma U_{ab}(90°)$
(c) Difference image $\Sigma U_{ab}(0°)$-$\Sigma U_{ab}(180°)$
(d) Difference image $\Sigma U_{ab}(0°)$-$\Sigma U_{ab}(270°)$

Fig. 8 shows the distance image without motion compensation using the pseudo 4-phase shift algorithm. Again it can be seen that the distance at the object edges are not calculated correctly (area 1 and area 3) and that the standard deviation is larger than in the other areas (see table 2). However the distorted edges are smaller as only two image captures are needed to calculate the distance. It can be also noticed that the distance image in Fig. 8 (a) is noisier than in Fig. 8 (b) due to the calibration method proposed in (Hussmann et al., 2011a).
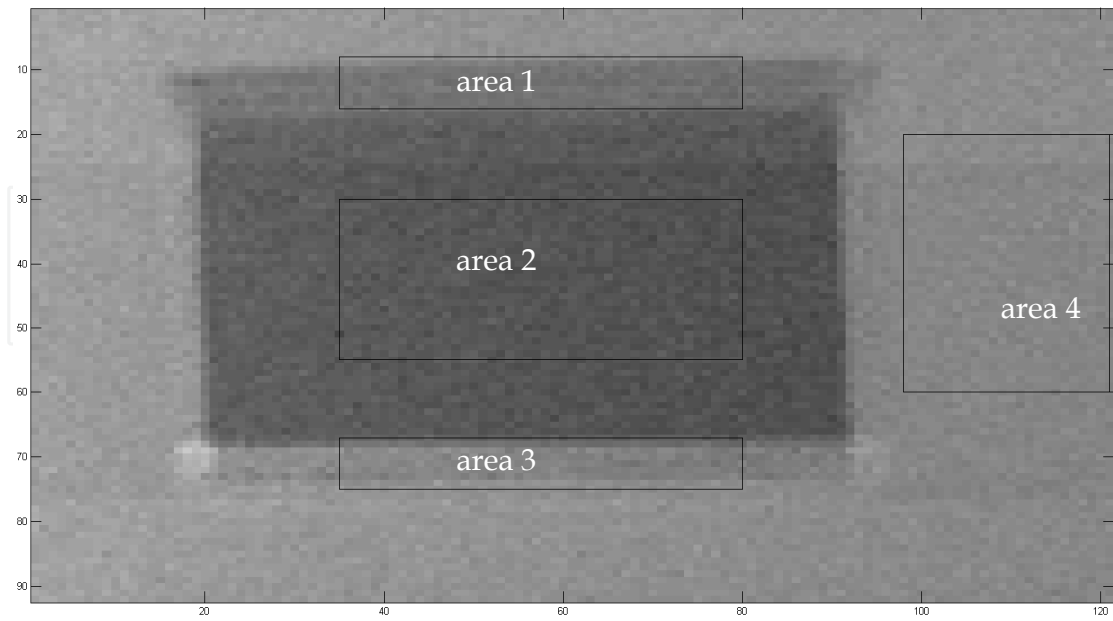
(a)
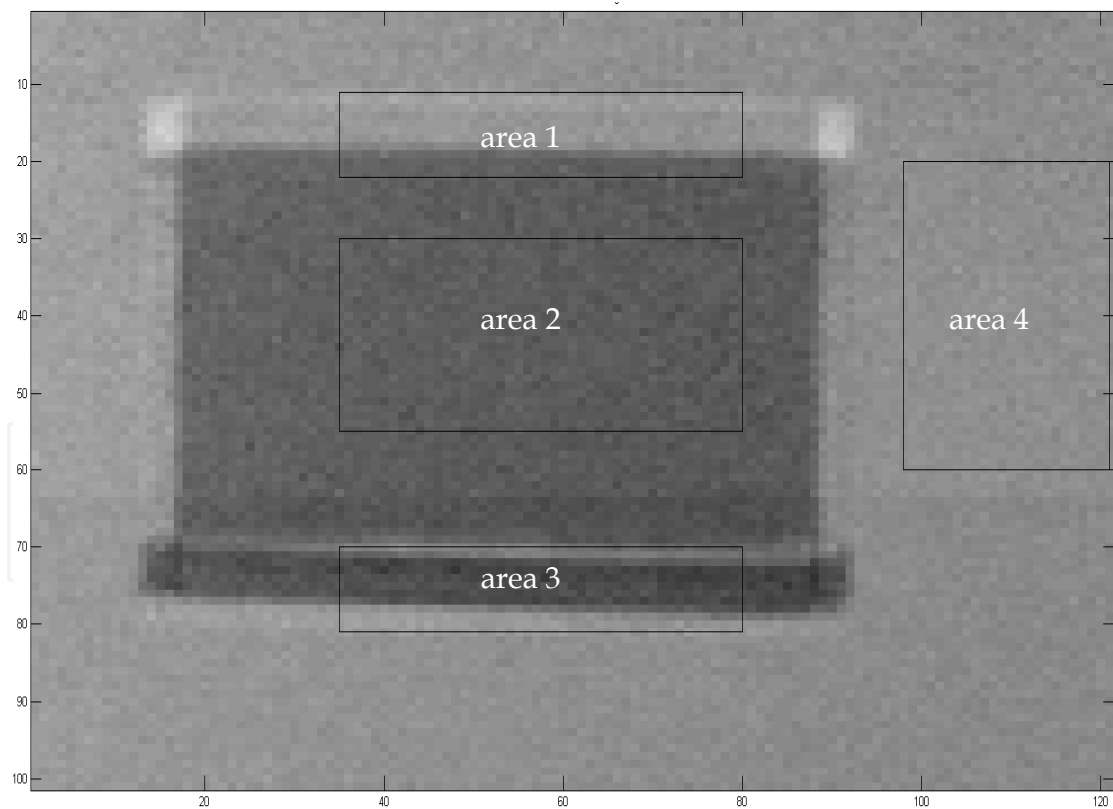
(b)

Fig. 7. Distance image using state-of-the-art 4-phase shift algorithm without calibration (a) and with calibration (b).
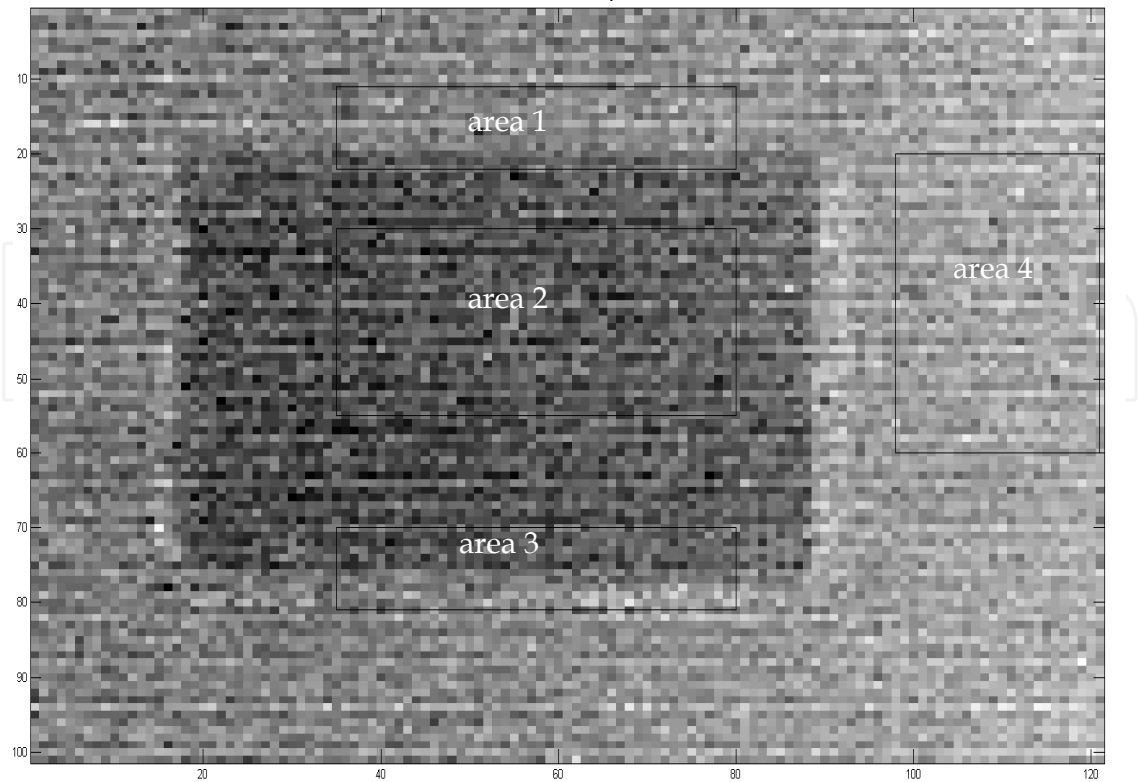
(a)
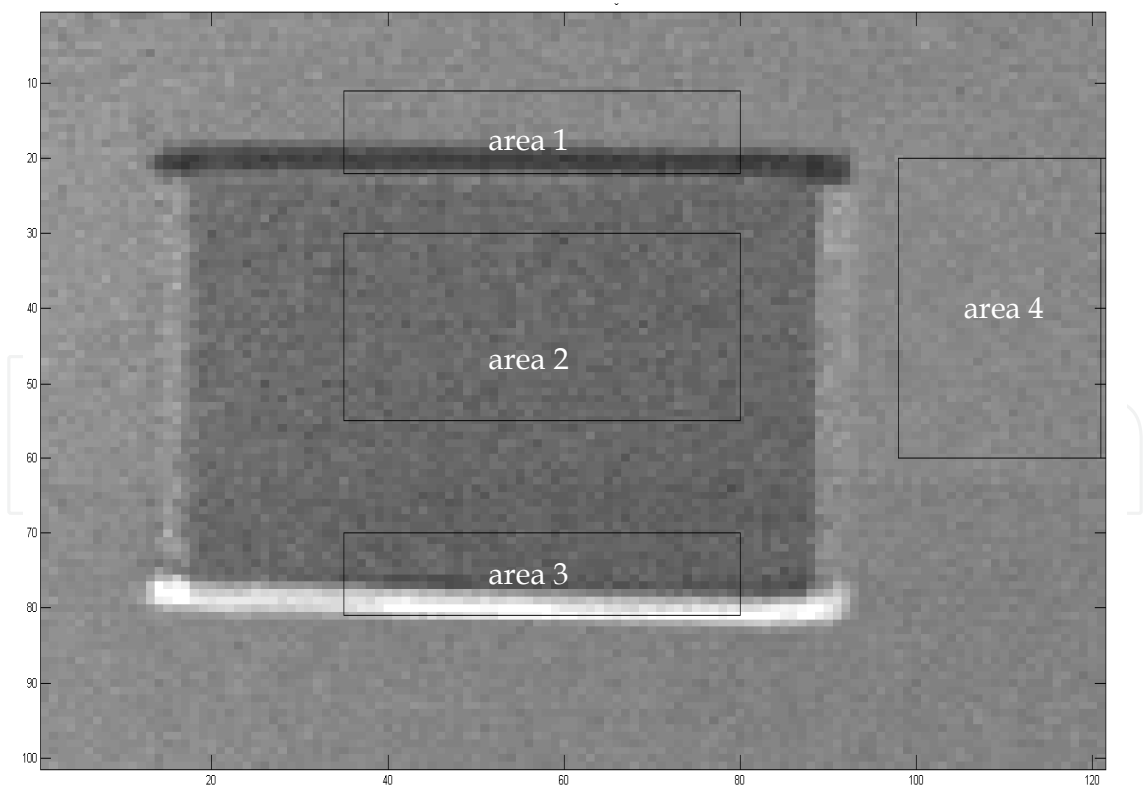
(b)

Fig. 8. Distance image using pseudo 4-phase shift algorithm without calibration (a) and with calibration (b).

Fig. 9 shows the distance image with motion compensation using the 4-phase shift algorithm. The distance image has clear edges without any distance uncertainties and the object dimensions can be calculated correctly. However it can be noticed again that the distance image in Fig. 9 (a) is noisier than in Fig. 9 (b) due to the calibration method proposed in (Hussmann et al., 2011a).
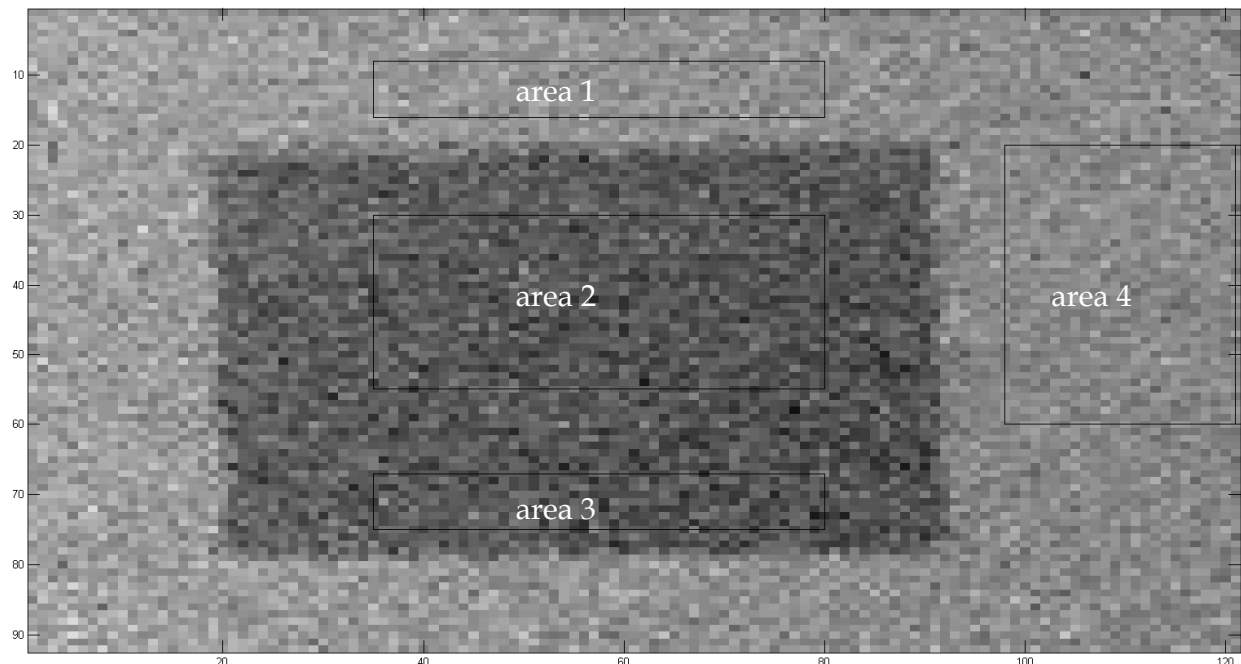

(a)
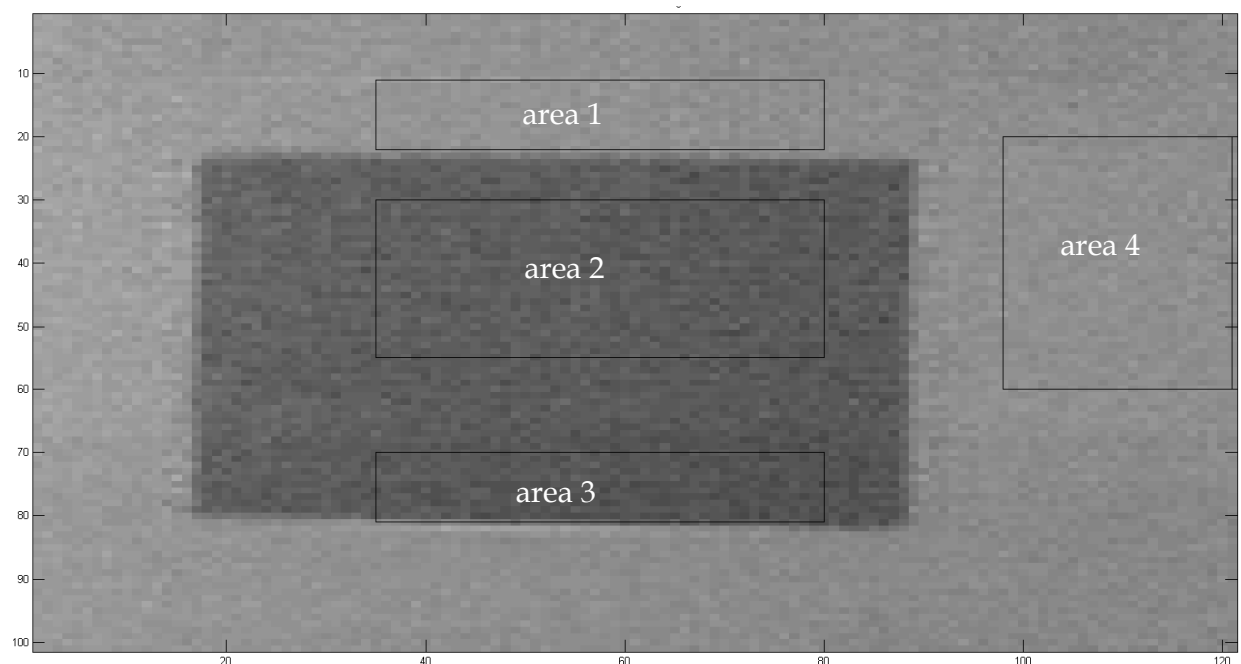
(b)

Fig. 9. Distance image using motion compensation algorithm based on the 4-phase shift algorithm without calibration (a) and with calibration (b).

Fig. 10 shows the distance image with motion compensation using the pseudo 4-phase shift algorithm. The distance image has also clear edges without any distance uncertainties and the object dimensions can be calculated correctly. However it can be noticed again that the distance image in Fig. 10 (a) is noisier than in Fig. 10 (b) due to the calibration method proposed in (Hussmann et al., 2011a).
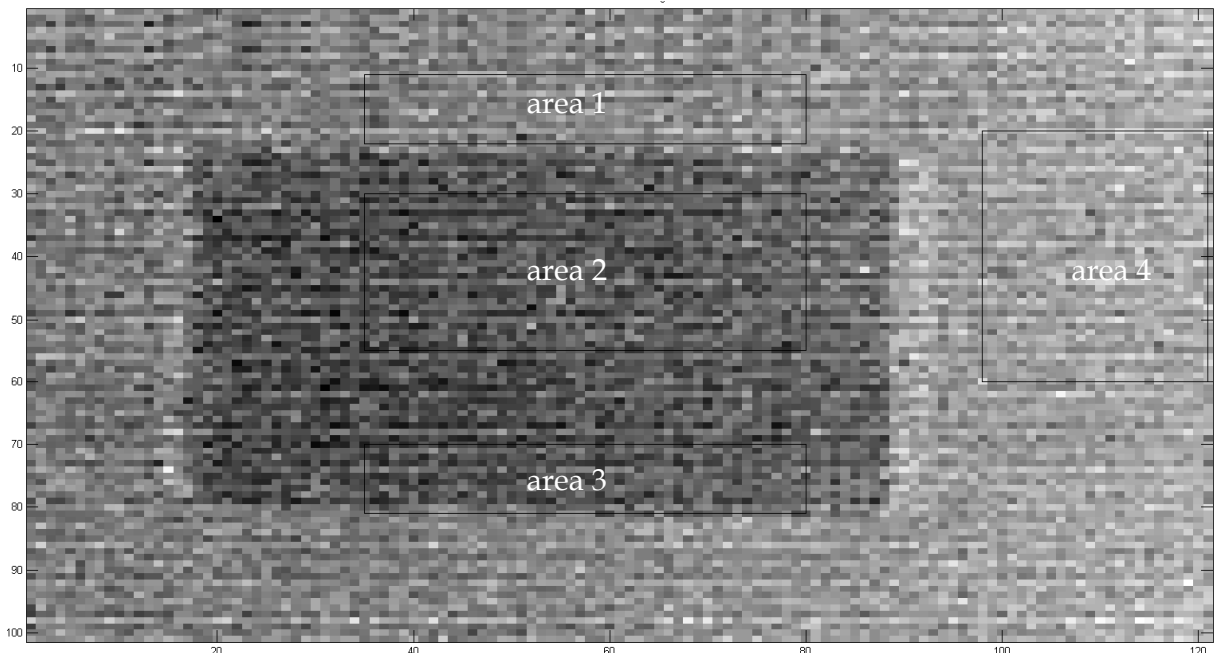
(a)
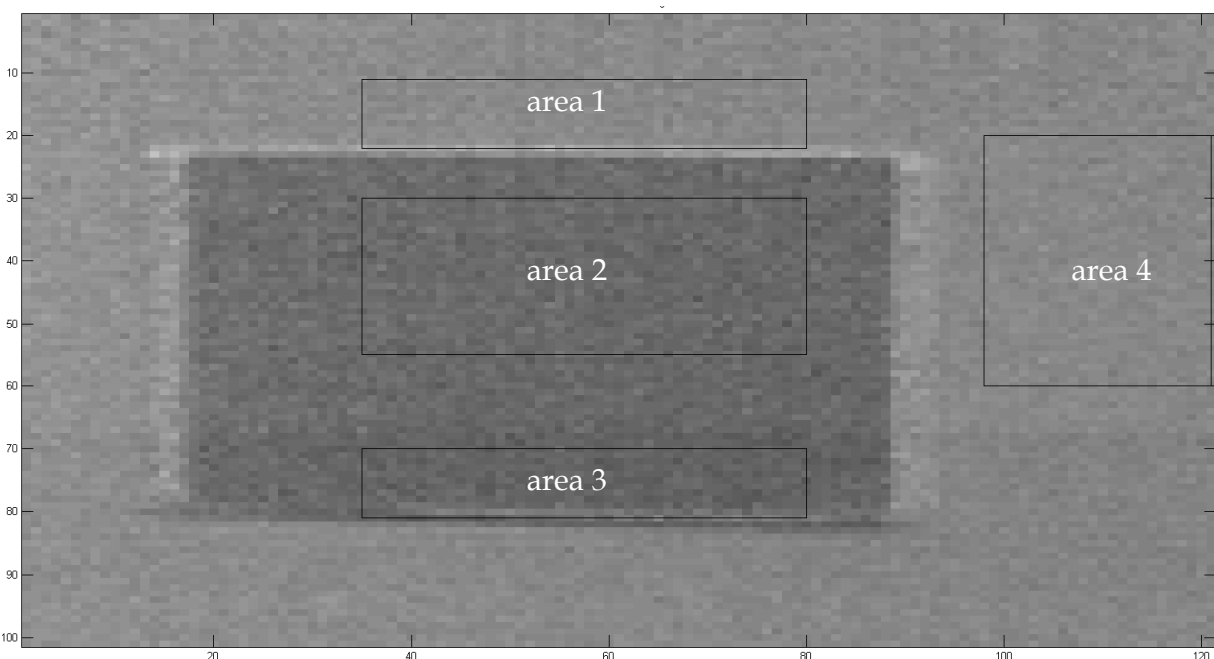
(b)

Fig. 10. Distance image using motion compensation algorithm based on the pseudo 4-phase shift algorithm without calibration (a) and with calibration (b).

Distance image (marked area)	Mean value and Standard deviation in cm			
	State-of-the-art 4-phase shift algorithm	*Pseudo 4-phase shift algorithm*	*Motion compensation algorithm (4-phase shift algorithm)*	*Motion compensation algorithm (pseudo 4-phase shift algorithm)*
area 1 uncalibrated	100.2/1.8	99.0/4.5	104.5/2.3	100.7/4.2
area 1 calibrated	102.0/3.9	127.6/4.4	104.2/0.8	131.0/1.4
area 2 uncalibrated	95.1/0.8	93.1/4.5	95.4/2.7	93.1/4.3
area 2 calibrated	95.5/0.8	125.9/1.0	95.8/0.9	125.8/0.9
area 3 uncalibrated	101.6/2.4	96.6/5.7	95.3/3.0	93.7/4.4
area 3 calibrated	97.5/5.1	130.3/9.0	95.1/1.6	125.2/1.4
area 4 uncalibrated	102.7/0.6	104.9/3.7	103.1/2.2	105.1/3.8
area 4 calibrated	103.5/0.6	130.7/0.7	103.7/0.6	130.5/0.7

Table 2. Spatial noise of the distance images in Fig. 7 – Fig. 10

The mean value and standard deviation across all pixels within the marked areas in Fig. 7 – Fig. 10 has been calculated and the results are shown in table 2. It can be clearly seen that the proposed motion compensation algorithm (with calibration) in (Hussmann et al., 2011a) combined with the pseudo-four-phase-shift algorithm proposed in (Hussmann & Edeler, 2010) has almost the same standard deviation for the background (area 4) and the object (area 2) as the state-of-the-art 4-phase shift algorithm and the motion compensation algorithm (with calibration) in (Hussmann et al., 2011a). However the mean value of the proposed motion compensation algorithm (with calibration) has an offset due to the calibration. Hence this offset has to be calibrated as well. Anyhow the proposed combination algorithm is working at the double frame rate, which is a desired feature for machine vision applications.

4. Conclusion

In this chapter we highlighted the advantages of the PMD technology for machine vision applications compared to other range measurement systems. The equations needed for the design of such a system are derived and demonstrate the simplicity of the extraction of the range information. A PMD camera delivers absolute geometrical dimensions of objects

without depending on the object surface, - distance, -rotation and –illumination. Hence PMD TOF vision systems are rotation-, translation- and illumination invariant.

The major advantage of the PMD technology is the delivery of an evenly distributed range and intensity images because each pixel calculates a range and intensity value. The PMD technology has an inherent suppression of uncorrelated light signals such as sun light or other modulated light disturbances. However if those light sources saturate the sensor, the range information is lost. More advantages of the PMD technology are the acquisition of the intensity and range data in each pixel without high computational cost and any moving components as well as the monocular setup. All these advantages lead to a compact and economical design of 3D TOF vision system with a high frame rate. This vision system can not only be used for machine vision applications but also for many other applications such as robotic, automotive, medical and multimedia applications.

In this chapter experimental results of a modified motion artefact compensation algorithm for PMD TOF vision system for a typical machine vision application are presented. Distance uncertainties at the object edges are greatly reduced. However a calibration (multiplicative shading correction) has to be done before to achieve this performance. The experimental results show that the proposed modified algorithm is working at the double frame rate compared to the original motion artefact compensation algorithm with almost the same performance. For real-time machine vision applications it is very important to have a high frame rate. The proposed algorithm will be more suited as only two image captures are needed instead of four to calculate the distance image.

The aim of the proposed motion compensation algorithm is to remove the displacement between the same target object points in the amplitude images due to the target movement. Subsequently the compensated amplitude images are used to calculate the distance image. Hence the target object must not have a uniformly reflecting surface. For the same reason the object orientation or form also does not affect the performance of the proposed algorithm.

It has to be noticed that the proposed modified motion artefact compensation algorithm (and also the original algorithm) only works for constant lateral movements. Speed changes are not taken into account, which would result in distance uncertainties at the object edges. But still the proposed method is able to determine the 3D dimension measurement of fast moving objects with a higher precision than the state-of-the art 4-phase-shift algorithm.

The performance of the proposed modified motion artefact compensation algorithm is investigated offline using Matlab. It has been shown that the algorithm is working at the double frame rate compared to the original motion artefact compensation algorithm. The maximum frame rate of the used commercial camera (PMD[vision]® CamCube 2.0) is 25 fps, which corresponds to a capture time of 40 ms per image. If the proposed algorithm would be implemented into the PMD camera, the frame rate would increase to 50 fps and a capture time of 20 ms respectively. If the hardware arctangent function in section 2.4, which has a total processing time for one range image of 6.66 ms, would be implemented as well, there would be 13.34 ms left for the remaining processing. This time is long enough to calculate

the range data in real-time. Hence it can be concluded that the proposed algorithms are well suited for machine vision applications.

5. Acknowledgment

6. References

Blanc, N., Oggier, T., Gruener, G., Weingarten, J., Codourey, A. & Seitz, P. (2004). Miniaturized smart cameras for 3D-imaging in real-time, *Proc. of the IEEE Sensors*, vol.1, pp. 471-4

Hu, G. & Stockman, G. (1989). 3-D Surface Solution Using Structured Light and Constraint Propagation, *IEEE Trans. Pattern Anal. Machine Intell.*, 11(4), pp. 390-402

Hussmann, S. & Hess, H. (2006). Dreidimensionale Umwelterfassung, *Trade Journal: "Elektronik automotive"*, WEKA Publisher House, Issue 8, ISSN 1614-0125, pp. 55-59

Hussmann, S., Ringbeck, T. & Hagebeuker, B. (2008). A performance review of 3D TOF vision systems in comparison to stereo vision systems, In: *Stereo Vision* (Online book publication), I-Tech Education and Publishing, Vienna, Austria, ch. 7, ISBN 978-953-7619-22-0, pp. 103-120

Hussmann, S. & Liepert, T. (2009). 3D-TOF Robot Vision System, *IEEE Trans. on Instrumentation and Measurement,* 58(1), pp. 141-146

Hussmann, S. & Edeler, T. (2010). Pseudo 4-phase shift algorithm for performance enhancement of 3D-TOF vision systems, *IEEE Trans. on Instrumentation and Measurement,* 59(5), pp. 1175-1181

Hussmann, S., Hermanski, A. & Edeler, T. (2011). Real-Time Motion Artifact Suppression in TOF Camera Systems, *IEEE Trans. on Instrumentation and Measurement,* 60(5), pp. 1682-1690

Hussmann, S., Knoll, F. & Edeler, T. (2011). Real-time image Processing of TOF range images using a reconfigurableprocessor system, *Proc. SPIE Vol.8085, Videometrics, Range Imaging and Applications XI*, pp. 808507 (8)

Jarvis, R. A. (1983). A perspective on range finding techniques for computer vision, *IEEE Trans. Pattern Anal. Machine Intell.*, 5(2), pp. 122-139

Lange, R. & Seitz, P. (2001). Solid-state time-of-flight range camera, *IEEE Journal of Quantum Electronics*, vol. 37, no. 3, pp. 390–397

Nuechter, A., Surmann, H. & Hertzberg, J. (2003). Automatic model refinement for 3D reconstruction with mobile robots, *Proc. of the 4th IEEE Intl. Conference on Recent Advances in 3D Digital Imaging and Modeling*, pp. 394–401

PMD Technologies, http://pmdtec.com (last accessed August 2011)

Ringbeck, T. & Hagebeuker, B. (2007). A 3D Time of flight camera for object detection, *Proc. of the 8th Conf. On Optical 3-D Measurement Techniques*, Zürich, Online-publication:

(http://www.pmdtec.com/fileadmin/pmdtec/downloads/publications/200705_P MD_ETHZuerich.pdf)

Schwarte, R., Xu, Z., Heinol, H., Olk, J., Klein, R., Buxbaum, B., Fischer H. & Schulte, J. (1997). New electro-optical mixing and correlating sensor: facilities and applications of the photonic mixer device (PMD), *Proc. SPIE, vol. 3100,* pp. 245-53
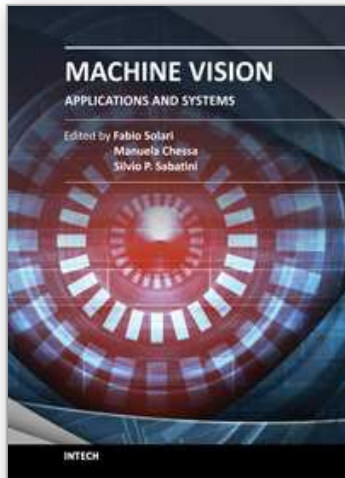
Machine Vision - Applications and Systems

Edited by Dr. Fabio Solari

Vision plays a fundamental role for living beings by allowing them to interact with the environment in an effective and efficient way. The ultimate goal of Machine Vision is to endow artificial systems with adequate capabilities to cope with not a priori predetermined situations. To this end, we have to take into account the computing constraints of the hosting architectures and the specifications of the tasks to be accomplished, to continuously adapt and optimize the visual processing techniques. Nevertheless, by exploiting the low?cost computational power of off?the?shell computing devices, Machine Vision is not limited any more to industrial environments, where situations and tasks are simplified and very specific, but it is now pervasive to support system solutions of everyday life problems.

How to reference

In order to correctly reference this scholarly work, feel free to copy and paste the following:

INTECH
open science | open minds